Photoelectron Spectra, Ab Initio SCF MO, and Natural Bond Orbital Studies on Stellenes. Long-Range π/σ Interactions

Rolf Gleiter,* Holger Lange, and Oliver Borzyk

Contribution from the Organisch-Chemisches Institut der Universität Heidelberg, Im Neuenheimer Feld 270, D-69120 Heidelberg, Germany

Received December 18, 1995[⊗]

Abstract: The He I photoelectron spectra of 2,6-dimethylenetricyclo[3.3.0^{1,5}.0^{3,7}]octane, (stella-2,6-diene) (**6**), stella-2,6-dione (**8**), stella-6-en-2-one (**10**), distella-2,2′,6,6′-triene (**7**), distella-6,6′-en-2,2′-dione (**9**), and distella-2,2′,6′-dien-6-one (**11**) have been recorded. The energy differences between the π ionizations arising from the terminal π bonds amount to 0.9 eV (**6**) and 0.4 eV (**7**). An energy difference of 1.1 eV has been found between the 2p lone-pair ionizations of **8**. Using Hartree−Fock SCF calculations with a 3-21G basis, the geometries of **6**−**11** have been calculated. For all six molecules long central σ bonds (1.58−1.60 Å) were predicted. By means of the Weinhold natural bond localization procedure, the interactions between the σ frame and the π orbitals as well as between the σ frame and the n orbitals have been probed. It has been concluded that the large energy splitting between the π MOs mainly localized at the terminal π bonds in **6** and **7** is mediated by the ribbon orbitals of the twisted cyclohexane ring.

Introduction

The possible interactions between two π systems can be subdivided into conjugation, homoconjugation, spiroconjugation, and through-bond interaction. We use the notion of conjugation if both π fragments are connected by one σ bond (**A**), while the term homoconjugation is used if the π fragments are held in close proximity by one or two sp^3 centers (**B**). In the case of spiroconjugation, both π fragments are held perpendicular to each other by a sp^3 center in such a way, that a favorable overlap between the two sets of orbitals is possible (**C**).

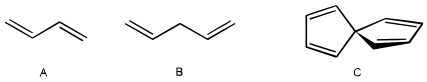

Common to all three bonding situations is a sizeable spatial overlap of the π fragments. Besides **A**−**C** there is also the possibility that the π orbitals interact via the σ system. This was first pointed out and analyzed by Hoffmann.[1] The through-bond coupling has been suggested to be responsible for long-range intramolecular electron and energy transfers between different chromophores.[2] In several model studies it has been shown that the interaction between π and σ systems depends on the length and nature of the σ chain between the π units. Striking examples have been found through comparison of the interactions between the two triple bonds in cycloocta-1,5-diyne (**1**),[3a] cyclodeca-1,6-diyne (**2**),[3b] and 3,3,4,4,7,7,8,8-octamethyl-3,4,7,8-tetrasilacycloocta-1,5-diyne (**3**).[3c] He I photoelectron (PE) spectroscopy has revealed that the energy differences of those vertical ionization energies, $I_{v,j}$ which are assigned to the ionizations from the in-plane bonding (π_i^+) and antibonding (π_i^-) linear combinations of the π bonds, depend strongly on the chain length and the nature of the σ bond and not so much on the distance between the triple bonds (Figure 1). A second example concerns the interaction of the π systems in **4** and **5**. In the case of **4**, the relay is the σ system of the central cyclobutane moiety,[4] while in **5**, it is the bicyclo[1.1.1]pentane cage system[5] (Figure 2a).

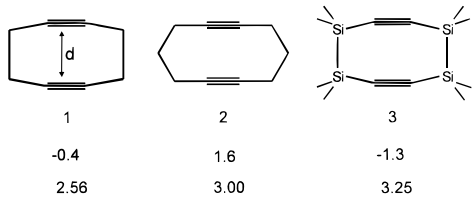

Figure 1. Measured energy difference of the vertical ionization energies, $I_{v,j}$, assigned to the ionizations from the in-plane π orbitals (π_i^-, π_i^+) and the distance, *d*, between the triple bonds.

In the framework of perturbation theory,[6] the following prerequisites for a sizeable (and measurable) interaction between π and σ systems can be formulated: (i) similar basis orbital energies of the interacting molecular fragments and (ii) the linear combinations of the π MOs and the σ MOs of the central molecular fragment must belong to the same irreducible representation. These two requirements are met in the case of **4** and **5**. The basis orbital energies of the Walsh-type orbitals

[⊗] Abstract published in *Advance ACS Abstracts,* May 1, 1996.

(1) Hoffmann, R.; Imamura, A.; Hehre, W. J. *J. Am. Chem. Soc.* **1968**, *90*, 1499. Reviews: Hoffmann, R. *Acc. Chem. Res.* **1971**, *4*, 1. Gleiter, R. *Angew. Chem., Int. Ed. Engl.* **1974**, *13*, 696. Paddon-Row, M. N. *Acc. Chem. Res.* **1982**, *15*, 245. Paddon-Row, M. N.; Jordan, K. D. In *Modern Models of Bonding and Delocalization*; Liebman, J. F., Greenberg, A., Eds.; Verlag Chemie: Weinheim, Germany, 1988; p 115. Martin, H. D.; Mayer, B. *Angew. Chem., Int. Ed. Engl.* **1983**, *22*, 283. Gleiter, R.; Schäfer, W. *Acc. Chem. Res.* **1990**, *23*, 369. Eckert-Maksic, M. In *Theoretical Models of Chemical Bonding*; Maksic, Z. B., Ed.; Springer Verlag: Heidelberg, Germany, 1991; Part 3, p 153 and references therein.

(2) Closs, G. L.; Miller, J. R. *Science* **1988**, *240*, 440. Miller, J. R. *Nouv. J. Chem.* **1987**, *11*, 83. Wasielewski, M. R. *Chem. Rev.* **1992**, *92*, 435. Jordan, K. D.; Paddon-Row, M. N. *Chem. Rev.* **1992**, *92*, 395 and references therein.

(3) (a) Bieri, G.; Heilbronner, E.; Kloster-Jensen, E.; Schmelzer, A.; Wirz, J. *Helv. Chim. Acta* **1974**, *57*, 1265. (b) Gleiter, R.; Karcher, M.; Hahn, R.; Irngartinger, H. *Chem. Ber.* **1988**, *121*, 735. (c) Gleiter, R.; Schäfer, W.; Sakurai, H. *J. Am. Chem. Soc.* **1985**, *107*, 3046.

(4) Gleiter, R.; Toyota, A.; Bischof, P.; Krennrich, G.; Dressel, J.; Pansegrau, P. D.; Paquette, L. A. *J. Am. Chem. Soc.* **1988**, *110*, 5490.

(5) Gleiter, R.; Pfeifer, K. H.; Szeimies, G.; Bunz, K. *Angew. Chem., Int. Ed. Engl.* **1990**, *29*, 413.

(6) Heilbronner, E.; Bock, H. *Das HMO-Modell und seine Anwendung*, Verlag Chemie, Weinheim, Germany, 1968. Dewar, M. J. S.; Dougherty, R. C. *The PMO Theory of Organic Chemistry*; Plenum Press: New York, 1975.

S0002-7863(95)04237-5 CCC: $12.00

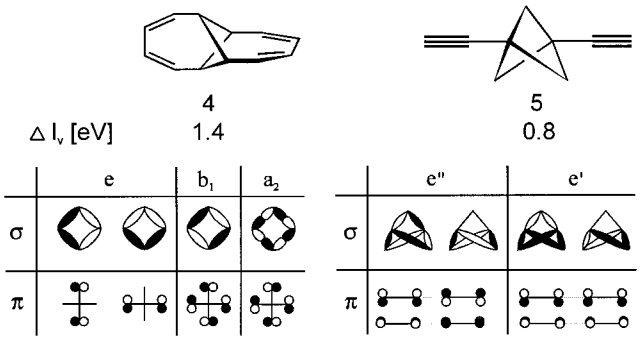

Figure 2. (a) Energy difference between the first two ionization energies of **4** and **5**. (b) Schematic display of relevant σ and σ^* orbitals of a four-membered ring with the π MOs of tricyclo[5.5.0.$0^{2,8}$]-dodecatetraene (left) as well as the σ MOs of bicyclo[1.1.1]butane and the π MOs of two triple bonds (right).

of cyclobutane[7] and bicyclo[1.1.1]pentane[5] are close to the basis orbital energies of butadiene and acetylene, respectively. In both compounds the frontier orbitals of the σ and π systems belong to the same set of irreducible representations as shown in Figure 2b.

In this paper, we would like to point out that a six-membered ring, fixed in the twist conformation, can play the same role as a four-membered ring in **4**. The same holds true for the tricyclo-[3.3.0^{1,5}.0^{3,7}]octane (stellane)[8] and the bicyclo[1.1.1]pentane systems. The model compounds we would like to discuss are **6**−**11**. Here we describe the results of He I PE investigations

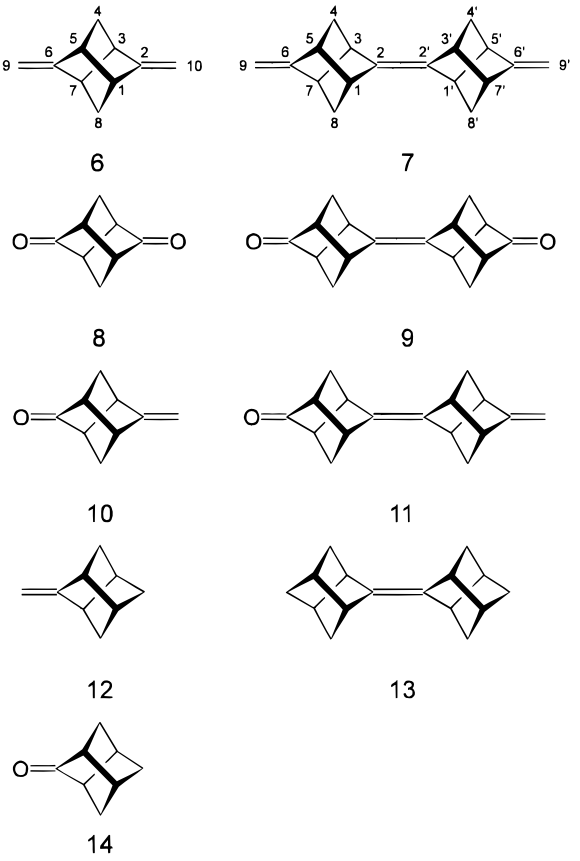

on these compounds.[9] These experimental studies are substantiated by the results of ab initio calculations on these molecules and our studies of the interaction of the π system with the σ frame using the Weinhold natural bond orbital (NBO) localization procedure.

Table 1. Vertical Ionization Energies (eV), $I_{v,j}$, and Calculated (3-21G Basis) Orbital Energies, $-\epsilon_j$, of **6**, **8**, **10**, and **12**−**14**

compd	band	$I_{v,j}$	assignment		$-\epsilon_j$ (3-21G)
12	1	8.96	15b	π	9.31
	2	10.20	14b	σ	11.12
13	1	7.90	$14b_2$	π	8.55
	2	8.70	$13b_2$	σ	10.40
14	1	8.76	15b	n	9.92
	2	10.90	14b	σ	12.02
6	1	8.49	$8b_2$	π	9.06
	2	9.40	$8b_3$	π	10.01
	3	10.05	$7b_2$	σ	11.07
8	1	8.84	$8b_2$	n	9.96
	2	9.90	$8b_3$	n	11.33
	3	11.58	$7b_2$	σ	12.74
10	1	8.85	15b	n	10.00
	2	9.40	16b	π	9.84
	3	10.95	20a	σ	12.29

Table 2. Vertical Ionization Energies (eV), $I_{v,j}$, and Calculated (3-21G Basis) Orbital Energies, $-\epsilon_j$, of **7**, **9**, and **11**

compd	band	$I_{v,j}$	assignment		$-\epsilon_j$ (3-21G)	
7	1	7.93	$15b_2$	π	8.49[a]	8.50[b]
	2	8.87	$14b_3$	π	9.45[a]	9.44[b]
	3	9.30	$14b_2$	π	9.91[a]	9.93[b]
	4	9.40	$13b_2$	σ	10.46[a]	10.41[b]
	5	10.27	$13b_3$	σ	11.54[a]	11.57[b]
9	1	8.63	$15b_2$	π	9.45	
	2	8.91	$14b_2$	n	9.90	
	3	9.02	$14b_3$	n	10.25	
	4	10.50	$13b_2$	σ	11.94	
11	1	8.34	29b	π	8.90	
	2	8.74	28b	n	9.84	
	3	9.34	27b	π	9.92	
	4	10.0	26b	σ	11.09	
	5	10.75	35a	σ	11.90	

[a] Orbital energies of the racemic form (D_2 symmetry, assignment according to this point group). [b] Orbital energies of the meso form (C_{2h} symmetry).

PE Spectra. The He I PE spectra of **6**−**11** are shown in Figures 3 and 5. The vertical ionization energies, $I_{v,j}$, are listed in Tables 1 and 2. Common to all three spectra in Figure 3 are bands with strong 0 ← 0 transitions below 10 eV, suggesting ionization events from nonbonding or weakly bonding orbitals, and bands with a Gaussian shape, indicating a geometrical change in the ionic state with respect to the ground state. To assign the bands to individual ionization processes we can proceed in one of two ways: Either in an empirical way, by comparing the bands with those of related species whose assignments are unequivocal such as **12**−**14**, or by comparing the ionization energies with the calculated canonical molecular orbital energies, $-\epsilon_j$, assuming that Koopmans' approximation[10] is valid for these species.

In Figure 4, the first PE bands of **12** and **14** are compared with those of **6**, **8**, and **10**. In going from **12** to **6**, the onset of the σ bands as well as the center of gravity of the π bands stays nearly constant. Therefore the assignment of the first three bands in the PE spectrum of **6** to ionization events from two π and one σ MO seems to be straightforward. Our qualitative assignment of the band sequence in the PE spectrum of **10** is based on the comparison between the PE data of **10** with those of **6** and **14** (Figure 4). The comparison with the PE spectrum of **14** shows the same position of the first bands and of the σ onset, suggesting the assignment of the first band in the PE spectrum of **10** to the ionization from the n orbital. In the

(7) Hoffmann, R.; Davidson, R. B. *J. Am. Chem. Soc.* **1971**, *93*, 5699. Salem. L.; Wright, J. S. *J. Am. Chem. Soc.* **1969**, *91*, 5947.

(8) Gleiter, R.; Kissler, B.; Ganter, C. *Angew. Chem., Int. Ed. Engl.* **1987**, *26*, 1252.

(9) Gleiter, R.; Borzyk, O. *Angew. Chem., Int. Ed. Engl.* **1995**, *34*, 1001.

(10) Koopmans, T. *Physica* **1934**, *1*, 104.

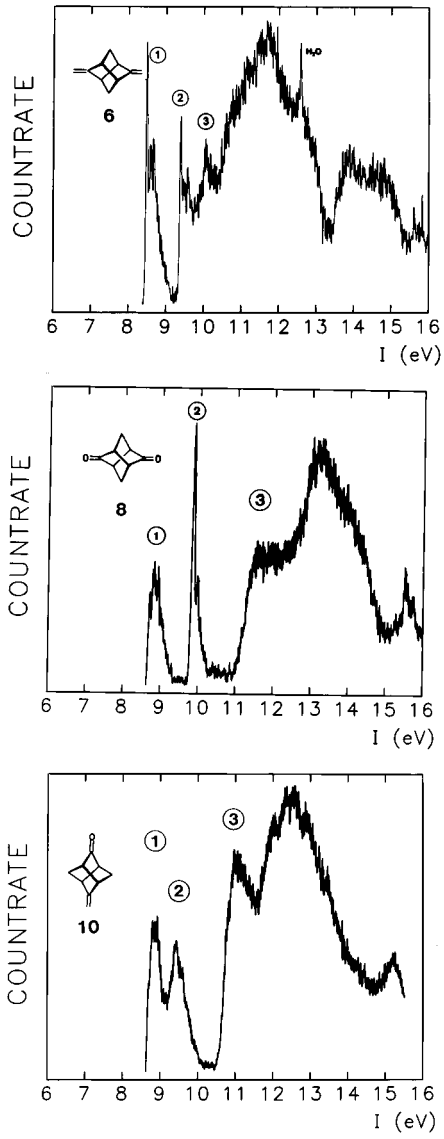

Figure 3. He I PE spectra of **6** (top), **8** (center), and **10** (bottom).

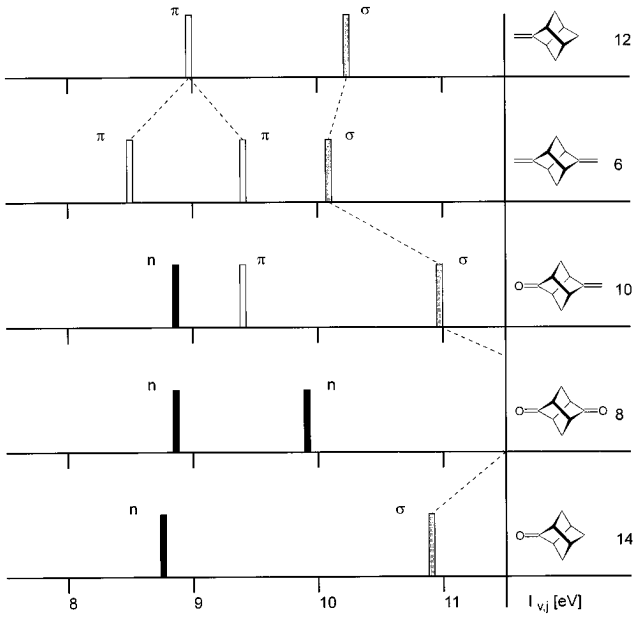

Figure 4. Correlation between the first ionization energies of **6**, **8**, and **10** with **12** and **14**, respectively.

comparison of the PE spectrum of **6** with that of **10** we have to take care of the higher electronegativity of oxygen with respect to carbon. As a rough measure, we can take the σ onset which is shifted toward a higher energy by 0.9 eV in going from **6** to **10**. If we consider this inductive shift of the center of gravity of the π bands of **6**, we predict a value for the π band around 10 eV. This suggests the assignment of the second band in the PE spectrum of **10** to the ionization event from the π MO. The assignment of the first two bands of the PE spectrum of **8** is straightforward from the comparison presented in Figure 4.

Our assignment of the band sequence in the PE spectra of **6** and **8** is further corroborated by Hartree−Fock SCF (HF-SCF) calculations using the split-valence 3-21G basis set.[11] As can be seen from Table 1, the calculated orbital sequence is in accordance with our empirical assignment given above. The recorded energy differences Δ between the first two ionization energies correspond well with the results of calculations: **6** (Δ exptl, 0.9 eV; Δ calcd, 1.0 eV), **8** (Δ exptl, 1.1 eV; Δ calcd, 1.4 eV). The sequence of the first two bands (n, π) in the PE spectrum of **10** given in Figure 4 differs from the result of HF-SCF calculations (Table 1). The calculations predict the orbital sequence π on top of n. Since the n orbital is usually strongly localized at the oxygen, we analyzed by ΔSCF (HF/6-31G*//HF/6-31G*) and ΔMP2 (MP2/6-31G*//HF/6-31G*) calculations whether or not this sequence is changed by Koopmans' defects, i.e. if it deviates from the $-\epsilon_j$ values. The ΔSCF calculations lead to an inverse order, n (7.85 eV) on top of π (8.06 eV). Taking into account correlation effects increases the energy of the ionization from the n and π orbitals (n, 8.00 eV; π, 9.29 eV). Both methods reveal a stronger Koopmans' defect for the n ionization and confirm the empirical assignment given in Figure 4. A more detailed analysis of the interactions in **6**−**8** and **10** will be provided below.

Note that the first two bands in the PE spectrum of **8** show rather different band shapes. While the band at 8.8 eV shows more of a Gaussian-type shape, the band at 9.9 eV exhibits a strong $0 \leftarrow 0$ transition. This difference points to a pronounced change in the geometry of the first ionic state, while for the second one, no such change occurs. This difference can usually be traced back to a stronger σ participation in the first case as compared to the second.

The PE spectra of **7** and **9** shown in Figure 5 result from mixtures of diastereomers (meso and enantiomers) which could not be separated (see also the Experimental Section). However, the calculations show only minor differences concerning the orbital energies of the diastereomers of either **7** and **9**. This is demonstrated in Table 2 for **7**.

The PE spectrum of **7** shows one peak at about 8 eV well separated from a broad peak between 9.0 and 9.5 eV. From the areas below the envelopes we can assign one ionization event to the first peak and three (bands 2−4) to the second. A comparison with the first ionization energy of **13** (7.9 eV) suggests that we must assign the first peak to the ionization from the π MO mainly localized at the central π bond (see Figure 6). The next two bands (8.9 and 9.3 eV) are assigned to the two linear combinations localized mainly at the terminal π bonds. This qualitative assignment is corroborated by comparing the center of gravity of the π bands of **6** (9.0 eV) with the center of gravity of bands 2 and 3 of **7** (9.1 eV).

The replacement of one exo-methylene group by an oxygen atom leads to a shift of the π ionizations to higher energies by 0.4−0.6 eV and also to an additional band around 9.0 eV which is assigned to the ionization of the 2p lone pair at the oxygen

(11) We used the Gaussian 92 program: Frisch, M. J.; Trucks, G. W.; Head-Gordon, M.; Gill, P. M. W.; Wong, M. W.; Foresman, J. B.; Schlegel, H. B.; Raghavachari, K.; Robb, M. A.; Binkley, J. S.; Gonzales, C.; Martin, R. L.; Fox, D. J.; Stewart, J. J. P.; Bobrowicz, F. W.; Rohlfing, C. W.; Kahn, L. R.; DeFrees, D. J.; Baker, J.; Pople, J. A. *Gaussian 92*; Gaussian Inc.: Pittsburgh, PA, 1992.

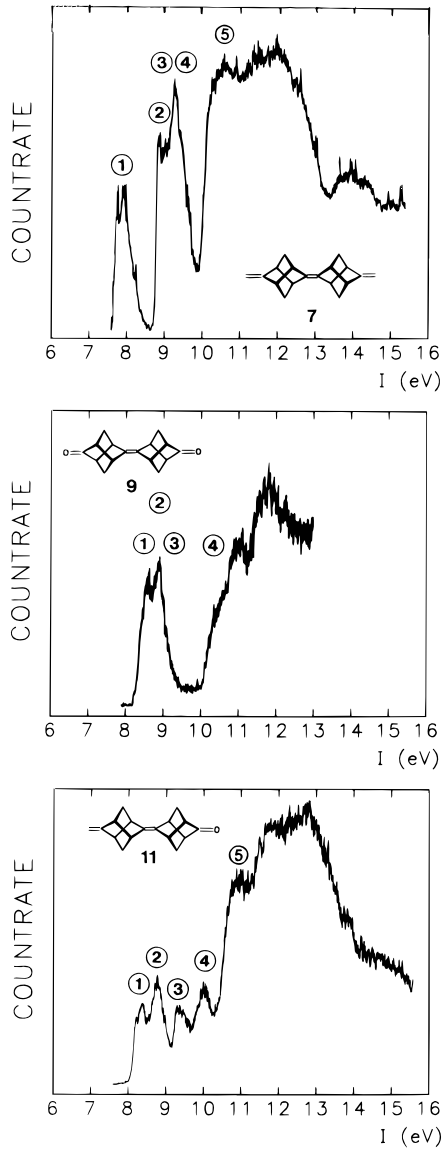

Figure 5. He I PE spectra of **7** (top), **9** (center), and **11** (bottom).

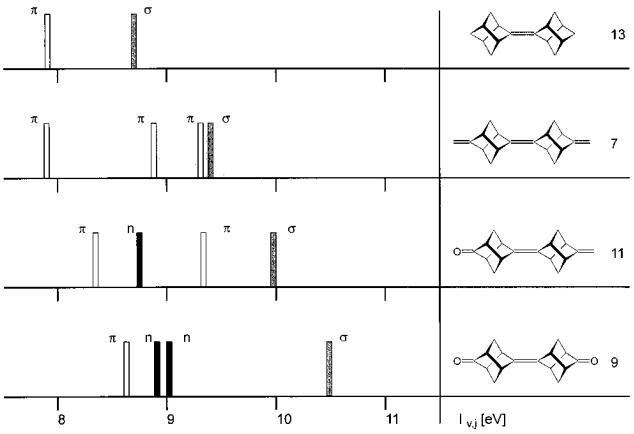

Figure 6. Correlation between the first ionization energies of **7**, **9**, and **11** with **13**.

center. This holds true as well for comparisons of the PE data of **7** and **11** (Figure 6). This situation leads to a splitting of the π bands in **11** by about 1 eV. A similar splitting was encountered in the PE spectrum of **6**. The dimer **9** can be derived from **7** by replacing both exo-methylene groups by one oxygen atom each. This replacement leads to a shift of the first π ionization energy by 0.7 eV toward higher energy and to a splitting of the two lone-pair ionizations by 0.1 eV. The qualitative assignments derived from the comparisons given in Figure 6 are confirmed by the results of SCF calculations as shown in Table 2.

Computations

A Methodology. The geometries of **6**−**11** were optimized at the Hartree−Fock level of theory using the split-valence 3-21G basis set.[11] Point group symmetries were D_2 for **6**−**9** and C_2 for **10** and **11**. The electronic structures of the six compounds were analyzed in terms of the through-space (TS)/through-bond (TB) concept developed by Hoffmann.[1] Here we make use of a methodology first suggested by Heilbronner and Schmelzer[12] which is based on the Fock matrix in a localized basis of the one-electron wave functions. The first step is the transformation of the canonical Hartree−Fock orbitals (CMOs) into a set of localized MOs by means of the Weinhold natural bond orbital localization procedure, which leads to the NBOs.[13] The matrix elements of the nondiagonal Fock matrix, $\mathbf{F}^{NBO}$, now have the following meanings: (1) The diagonal elements F_{ii}^{NBO} are the self-energies of the ith NBO ϕ_i. (2) The off-diagonal elements F_{ij}^{NBO} are a measure for the interaction energy between the NBOs ϕ_i and ϕ_j.

For a quantitative treatment, we apply the procedure of Imamura et al.,[14] which we will illustrate briefly. In order to calculate the TS interaction between the NBOs $\phi_1 - \phi_n$, one has to diagonalize the $[n \times n]$ submatrix of the $\mathbf{F}^{NBO}$ which includes all diagonal elements $F_{11}^{NBO}-F_{nn}^{NBO}$ and all off diagonal elements F_{ij}^{NBO}, $i \neq j = 1 \ldots n$. The eigenvalues of this $[n \times n]$ matrix are the energies after the TS interaction, and the corresponding eigenvectors are the so-called precanonical MOs (PCMOs).[12] Proceeding with the $[m \times m]$ submatrix in the same manner gives an illustration of the TB effect caused by the NBOs $\phi_{n+1}-\phi_m$. Notice that the $[m \times$ m$]$ matrix includes the $[n \times n]$ matrix. Now the eigenvalues are the energies after the TS interaction of $\phi_1-\phi_n$ and the TB interaction with $\phi_{n+1}-\phi_m$. Diagonalization of the complete $\mathbf{F}^{NBO}$ matrix leads to the CMOs in the basis of the NBOs. Our following discussion is based on the HF/3-21G calculations, unless stated otherwise.

Calculated Geometrical Parameters. Table 3 shows some of the structural parameters as obtained from the HF/3-21G geometry optimizations.

The most striking feature is the C_1-C_5 bond length. The elongation up to 1.592 −1.617 Å is due to the high strain energy caused by the rigid stellane frame. This is not an artifact of the 3-21G basis set. The calculated C_1-C_5 bond length of **8**, 1.592 Å, corresponds well with the value obtained by X-ray structure determination, 1.586 Å.[15] The shortening from 1.616 Å (**6**) to 1.604 Å (**10**) to 1.592 Å (**8**) correlates well with the increasing bond angles α(3,4,5) from 93,7° (**6**) to 94,1° (**10**) to 94.4° (**8**) and therefore can be traced back to the decreasing strain energy within the three molecules. The geometrical parameters listed in Table 3 are also fully in line with results from X-ray investigations on stelladienones.[16] These investigations revealed long central bonds (1.61−1.62 Å) and small angles at the sp^2 centers of the ring (96°−97°). The C−C bonds to the methylene bridges, d(1,8) and d(7,8), are also elongated, but the effect here is smaller than the effect on d(1,5). In the

(12) Heilbronner, E.; Schmelzer, A. *Helv. Chim. Acta* **1975**, *58*, 936.
(13) Reed, A. E.; Weinstock, R. B.; Weinhold, F. *J. Chem. Phys.* **1985**, *83*, 735. Reed, A. E.; Weinhold, F. *Ibid.* **1983**, *78*, 4066.
(14) Imamura, A.; Ohsaku, M. *Tetrahedron* **1981**, *37*, 2191. Using NBOs to analyze the TS/TB interaction: Liang, C.; Newton, M. D. *J. Phys. Chem.* **1992**, *96*, 2855. Naleway, C. A.; Curtiss, L. A.; Miller, J. R. *J. Phys. Chem.* **1991**, *95*, 8434. Paddon-Row, M. N.; Wong, S. S.; Jordan, K. D. *J. Am. Chem. Soc.* **1990**, *112*, 1710.
(15) Irngartinger, H.; Borzyk, O.; Gleiter, R. To be published.
(16) Siemund, V.; Irngartinger, H.; Sigwart, C.; Kissler, B.; Gleiter, R. *Acta Crystallogr.* **1993**, *C49*, 57.

Table 3. HF/3-21G-Optimized Geometrical Parameters for **6**−**11**[a]

parameter	**6**	**7**	**8**	**9**	**10**	**11**[b]
d(1−5)	1.616	1.617	1.592	1.604	1.604	1.605
						1.617*
d(1−2)	1.520	1.523	1.530	1.521	1.519	1.521
						1.523*
d(5−6)		1.520		1.530	1.530	1.530
						1.520*
α(1,2,3)	96.5	96.2	97.0	96.4	96.7	96.4
						96.2*
α(5,6,7)		96.4		96.8	96.9	96.8
						96.4*
α(3,4,5)	93.7	93.7	94.4	94.1	94.1	94.1
						93.7*
d(C═O)			1.201	1.202	1.203	1.203
d(C═O)						
(2−2′)		1.304		1.303		1.303
(6−9)	1.311	1.311			1.310	1.310*

[a] Bond lengths *d* are in Å, angles α are in degrees. For the atomic numbering, see formula, **6** and **7**. [b] * indicates that the primed numbers should be used, e.g. α(5′, 6′, 7′) instead of α(5, 6, 7).

case of the ketones (**8**−**10**), the small angle α(3,4,5) has an influence on the C═O bond length, which becomes shorter than that, for example, in acetone (1.211 Å).[17] The main reason for this is the diminished antibonding interaction between the n(2p)-orbital on oxygen and the coplanar σ bonds. Consequently, d(C═O) is shortened to 1.201 Å (**8**). The same holds true for the C═C bonds, with a value of 1.311 Å for the terminal bonds and 1.304 Å for the central bond (**7**). These distances are shorter than those in the comparable isobutene (1.318 Å).[17] The unexpectedly short central double bond convincingly shows that there is no significant steric repulsion between the two stellane units. This shortening can also be understood in terms of rehybridization. Forcing α(1,2,3) from the ideal sp^2 value of 120° down to nearly 90° induces a higher s character in the σ bond between C_2 and $C_{2'}$. The hybridization is given by the NBO analysis to be nearly $sp^{1.3}$, thus leading to bond shortening.

Analysis of π/σ Interactions in 6, 8, and 10. To understand the π/σ interactions in **6**−**11**, we will first consider the C,C σ orbitals of a twisted cyclohexane ring by means of the Weinhold natural bond localization procedure.[13] The resulting basis energies of the NBOs are shown on the left-hand side of Figure 7. The linear combination of the NBOs leads to the six PCMOs, which we will denote as ribbon orbitals[18] as shown at the right-hand side of Figure 7. Let us first focus on the $2b_2$ (σ) PCMO, for it fulfills the aforementioned conditions which are essential to a good relay effect: It has the proper symmetry (b_2) to interact with one of the π combinations as well as an energy (−13 eV) close enough to the π energy (−10 eV). In the case of $1b_3$ (σ), the interaction with the b_3 (π) PCMO is expected to be smaller due to the larger energy difference.

The interaction diagram for **6** is shown in Figure 8. The self-energies of the two π NBOs are on the left-hand side. The TS interaction leads to the corresponding PCMOs b_2 (π) and b_3 (π). The energy splitting is minute due to the large distance between both π bonds, $d(2-6) = 3.2$ Å. Nevertheless, using NBOs to analyze TB/TS interaction underestimates the TS effect.[19] The TB1 step shows the energetic influence of the ribbon orbitals (Figure 7). The interaction with $2b_2$ (σ) and $1b_3$ (σ) leads to considerable splitting due to the fact that, because $1b_3$ σ is considerably lower in energy than $2b_2$ (σ) (Figure 7), the interaction between $2b_2$ (σ) and b_2 (π) is more effective than the interaction $1b_3$ (σ) and b_3 (π).

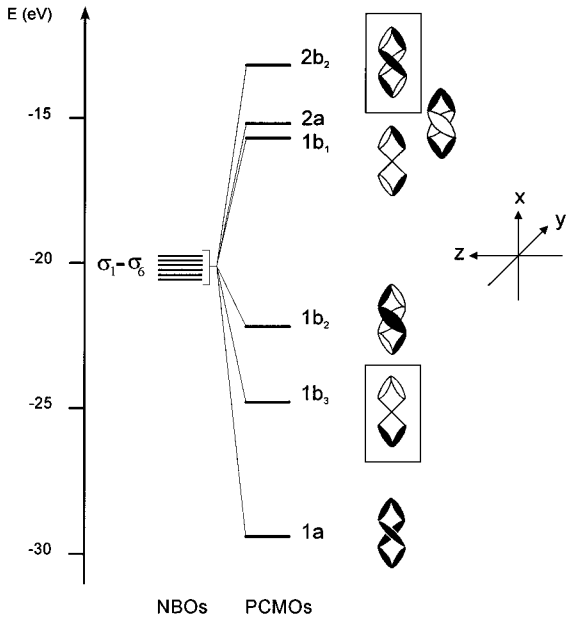

Figure 7. Transitions of the six degenerated NBOs of the C,C bonds (left) to the six precanonical (ribbon) orbitals (right) of a twisted cyclohexane ring.

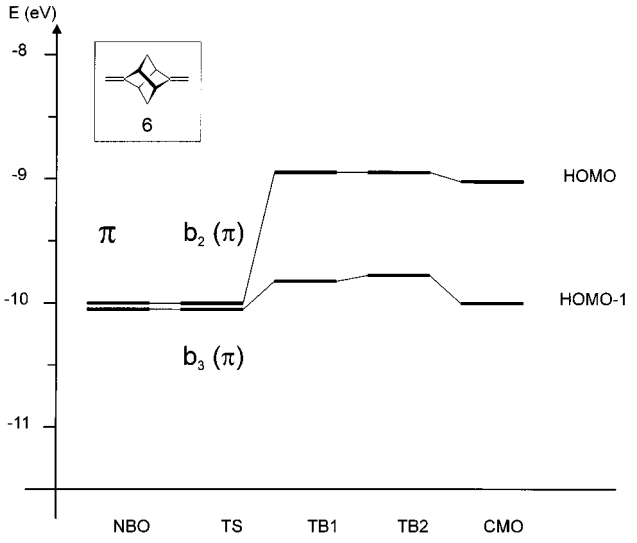

Figure 8. TS/TB interaction diagram of **6**: NBO, self-energy of the π NBOs; TS, energy after the TS interaction; TB1, energy after the interaction with the ribbon orbitals; TB2, energy after the interaction with the remaining σ_{CC} orbitals; CMO, energy of the CMOs.

The interaction of the 2p-type lone pairs at the oxygen atoms (b_3 (n) and b_2 (n)) with the ribbon orbitals of the central six-membered ring in **8** is minute (Figure 9, TB1). A strong interaction is encountered, however, if the C,C σ orbitals which connect the CO groups with the central ring (TB2) are considered. This result can also be interpreted in a different fashion: The stellane cage contains two twisted cyclohexane rings, the first one lying along the *x*-axis (*x*-ring) as shown in Figure 7. This ring is responsible for the interaction in **6**. A second ring is orientated in the *z*-direction (*z*-ring), and the ribbon orbitals formed by these six orbitals are responsible for the coupling between the lone pairs (indicated by the shaded boxes in Figure 10). The splitting of the two lone pairs is stronger because they are coplanar to the *z*-ring ribbon orbitals.

In view of the different shapes of bands 1 and 2 in the PE spectrum of **8** (see Figure 3), the ab initio calculations predict only small differences between the HOMO and HOMO-1, i.e. the HOMO shows 43% lone-pair character and 53% C,C σ participation, and the HOMO-1, 52% lone-pair character and

(17) Hehre, W. J.; Radom, L.; Schleyer, P. v. R.; Pople, J. A. *Ab initio Molecular Orbital Theory*; Wiley & Sons: New York, 1986.
(18) Hoffmann, R.; Mollère, P. D.; Heilbronner, E. *J. Am. Chem. Soc.* **1973**, *95*, 4860.
(19) Paddon-Row, M. N.; Wong, S. S.; Jordan, K. D. *J. Chem. Soc., Perkin Trans. 2* **1990**, 425.

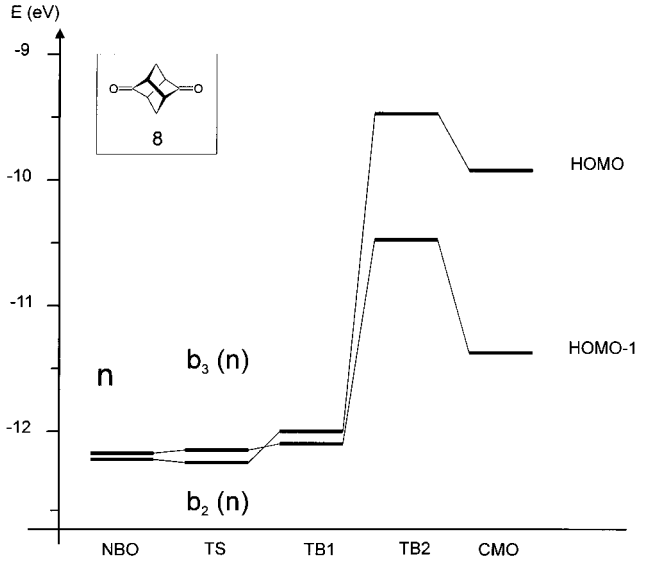

Figure 9. TS/TB interaction diagram of **8**: NBO, self-energy of the n NBOs; TS, energy after the TS interaction; TB1, energy after the interaction with the ribbon orbitals; TB2, energy after the interaction with the σ_{CC} orbitals; CMO, energy of the CMOs.

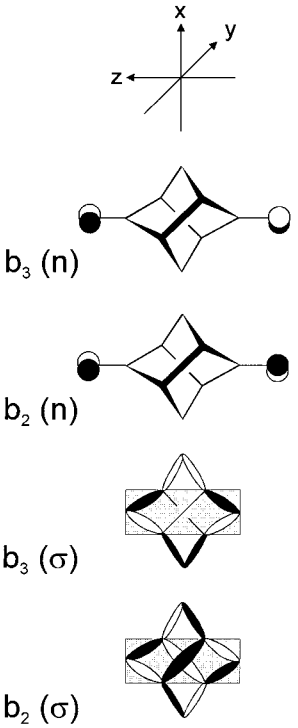

Figure 10. Schematic drawing of the PCMOs of the stellane skeleton (bottom) and of the lone pairs (top) of **8**.

34% C,C σ participation. The same analysis shows 80% π character and 20% C,C σ participation for the HOMO of **6**, while the HOMO-1 has 93% π character and only 4% participation of the ribbon orbitals.

In the case of **10**, both types of interaction, in which the ribbon orbitals of the *x*-ring as well as the PCMOs of the *z*-ring are used, are active in one molecule. The first set of orbitals interacts with the π MO and the second set with the n lone pair at the oxygen atom. Since the latter interaction is more effective than the *x*-ring interaction, very similar energies for the two highest occupied MOs in **10** result. This is demonstrated in Figure 11. At the TS level the energies for π and n remain unchanged. Both energy levels are separated by 1.35 eV. The *x*-ring ribbon orbitals (TB1) shift the π PCMO by about 0.8 eV up to −9.64 eV, whereas the b_2-like PCMO of the *z*-ring ribbon

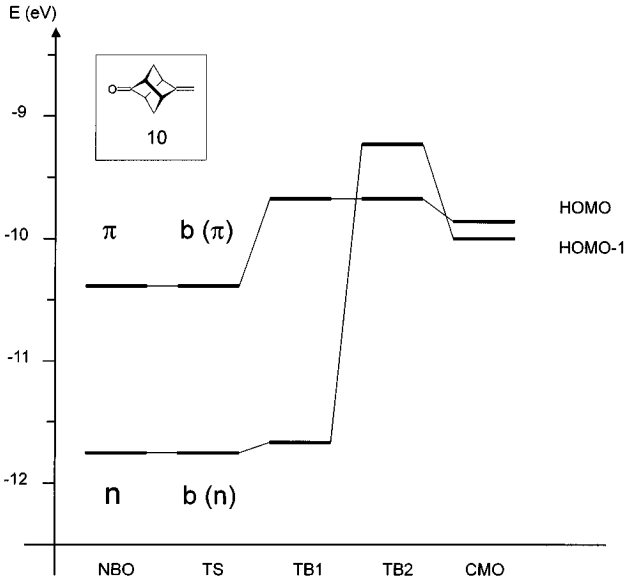

Figure 11. TS/TB interaction diagram of **10**: NBO, self-energy of the n and π NBOs; TS, energy after the TS interaction; TB1, energy after the interaction with the ribbon orbitals; TB2, energy after the interaction with the remaining σ_{CC} orbitals; CMO, energy of the CMOs.

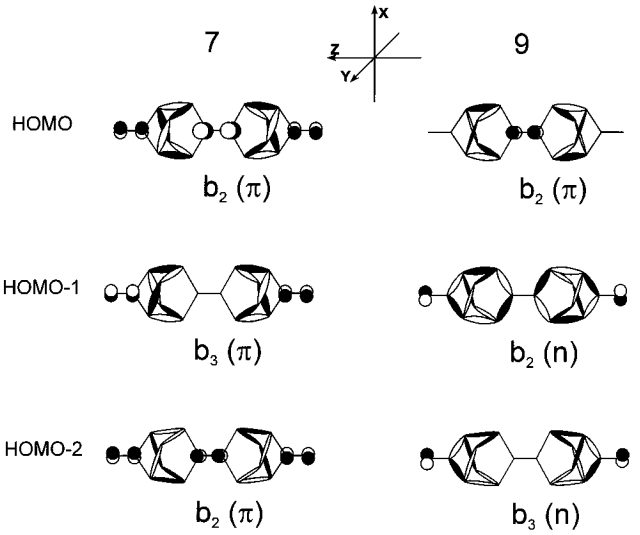

Figure 12. Schematic representation of the frontier orbitals (HOMO−HOMO-2) of **7** and **9**.

orbitals (TB2) shifts the n orbital by about 2.3 eV to −9.38 eV. As a result, both CMOs are energetically close together. A detailed analysis of the wave functions for the HOMO and HOMO-1, of **10** reveals 41% lone-pair character and 52% C,C σ participation for the HOMO-1, while 83% π character and only 16% σ character is computed for the HOMO.

Analysis of the π/σ Interaction in 7, 9, and 11. The dimers **7**, **9**, and **11** can be interpreted as being built out of their monomeric counterparts, i.e. **7**: **6** + **6**, **9**: **10** + **10**, and **11**: **6** + **10**. This analogy is also found in the geometric parameters (see Table 3), and it further holds true for the electronic structures of these dimers.

Although the π MOs in **7** are strongly influenced by the ribbon orbitals in the stellane fragment, they retain their "natural" order. This can best be seen from the wave functions of the three highest occupied MOs of **7** shown in Figure 12. In **9** the ribbon orbitals interact mainly with the central π MO, whereas the b_2(n) and b_3(n) combinations are mainly influenced by the C,C σ orbitals connecting the CO groups to the central six-membered rings. This is illustrated by the wave functions (Figure 12) and the interaction diagram shown in Figure 13.

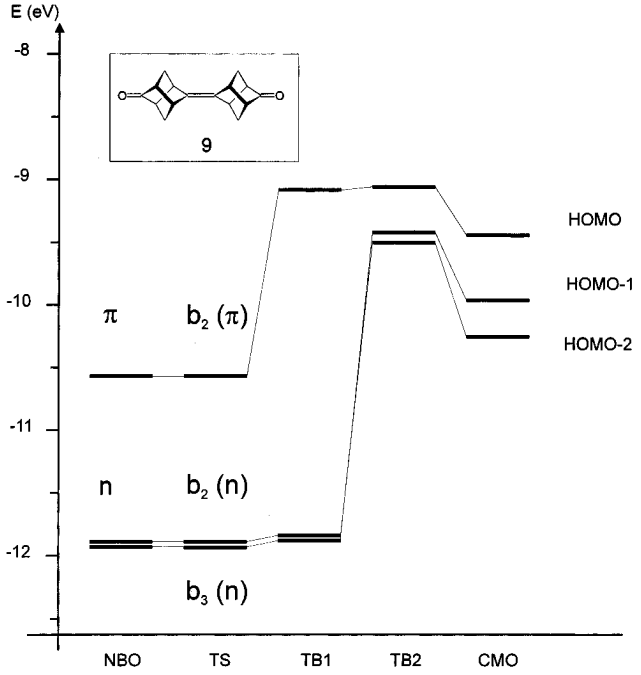

Figure 13. TS/TB interaction diagram of **9**: NBO, self-energy of the n and π NBOs; TS, energy after the TS interaction; TB1, energy after the interaction with the ribbon orbitals, TB2, energy after the interaction with the remaining σ_{CC} orbitals; CMO, energy of the CMOs.

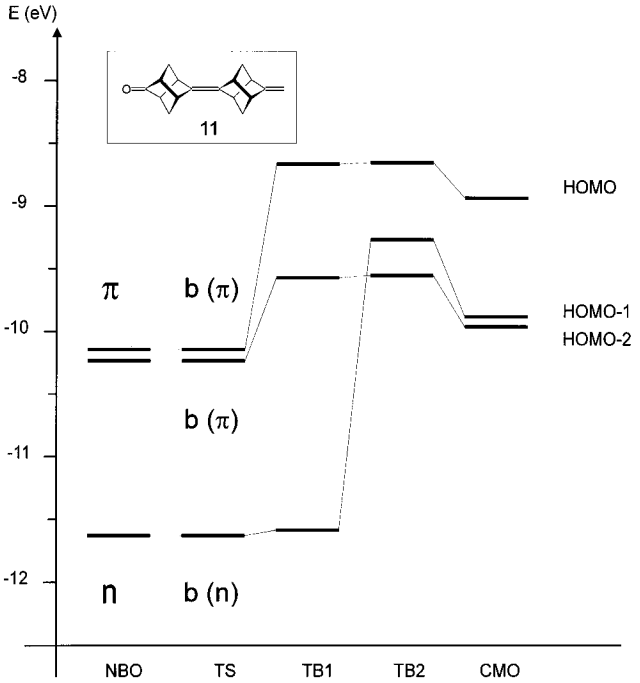

Figure 14. TS/TB interaction diagram of **11**: NBO, self-energy of the n and π NBOs; TS, energy after the TS interaction; TB1, energy after the interaction with the ribbon orbitals; TB2, energy after the interaction with the remaining σ_{CC} orbitals; CMO, energy of the CMOs.

The interaction diagram for **11** as shown in Figure 14 is also interesting. In the TB1 step, a stelladiene-type interaction is encountered. The ribbon orbitals of the stelladiene fragment spread the 29b(π) and 27b(π) PCMOs by 0.95 eV. When the C,C σ PCMOs adjacent to the CO group are taken into account in the second step, one observes destabilization of the lone pair by 2.3 eV.

Conclusions

Our PE investigations combined with quantum chemical analyses of **6**−**11** reveal a considerable splitting of both the nonconjugated π systems and 2p-type lone pairs. In the case of the monomeric species **6**, **8**, and **10**, we encountered a strong through-bond interaction, which in the case of **6** was caused by the central (*x*-ring) ribbon orbitals. In **8**, the interaction of the 2p lone pairs at the oxygens was strongly mediated by the *z*-ring ribbon orbitals, while in the case of **10**, both the *x*-ring and the *z*-ring acted as relays.

For the dimers **7**, **9**, and **11**, the strongest coupling is observed for the triene **7**. The π MOs reveal a "natural" sequence of the orbitals which is not caused by through-space interactions of the three double bonds but is instead mediated via the ribbon orbitals. If we consider the two stellane units and the central double bond as one relay system, this unit can be seen as a very effective system for long-range coupling. It leads to a 0.4 eV splitting of the MOs of the terminal π bonds. This is especially notable as the distance between them amounts to ca. 7 Å.

The splitting of the 2p lone pairs in **9** is relatively small (0.1 eV) compared to the large splitting in **8**. The main reason for this is that the central π bond cannot mediate the coupling due to its orthogonality to the relay orbitals of the two *z*-rings. Nevertheless, this might still be significant as the recorded splitting occurs despite a separation of 10 Å.

Experimental Section

The preparation of **6**−**11** and **13**[9,20,21] has been described in the literature. In the cases of **7** and **9**, we have not yet been able to separate the three stereoisomers (meso, racemate). The He I PE spectra were recorded on a Perkin Elmer PS18 spectrometer. The recording temperatures were as follows: **6**, 25 °C; **7**, 62 °C; **8**, 40 °C; **9**, 130 °C; **10**, 25 °C; **11**, 90 °C; **13**, 45 °C. The calibration was performed with Ar (15.76 and 15.94 eV) and Xe (12.13 and 13.44 eV). A resolution of 20 meV on the $^2P_{3/2}$ Ar line was obtained.

Acknowledgment. We thank A. Flatow for recording the PE spectra. We are grateful to the Deutsche Forschungsgemeinschaft, the Volkswagenstiftung, the Fonds der Chemischen Industrie, and the BASF Aktiengesellschaft for financial support. H.L. is grateful to the Studienstiftung des Deutschen Volkes for a graduate fellowship. This article is dedicated to Professor Edgar Heilbronner on the occasion of his 75th birthday.

JA954237K

(20) Kissler, B.; Gleiter, R. *Tetrahedron Lett.* **1985**, *26*, 185.
(21) Nakazaki, M.; Naemura, K.; Harada, H.; Narutaki, H. *J. Org. Chem.* **1982**, *47*, 3470.